

Changes in the halo formation rates due to features in the primordial spectrum

Dhiraj Kumar Hazra*

Harish-Chandra Research Institute Chhatnag Road,
Jhansi, Allahabad 211019, India

September 3, 2018

Abstract

Features in the primordial scalar power spectrum provide a possible roadway to describe the outliers at the low multipoles in the WMAP data. Apart from the CMB angular power spectrum, these features can also alter the matter power spectrum and, thereby, the formation of the large scale structure. Carrying out a complete numerical analysis, we investigate the effects of primordial features on the formation rates of the halos. We consider a few different inflationary models that lead to features in the scalar power spectrum and an improved fit to the CMB data, and analyze the corresponding imprints on the formation of halos. Performing a Markov Chain Monte Carlo analysis with the WMAP seven year data and the SDSS halo power spectrum from LRG DR7 for the models of our interest, we arrive at the parameter space of the models allowed by the data. We illustrate that, inflationary potentials, such as the quadratic potential with sinusoidal modulations and the axion monodromy model, which generate certain repeated, oscillatory features in the inflationary perturbation spectrum, do not induce a substantial difference in the number density of halos at their best fit values, when compared with, say, a nearly scale invariant spectrum as is generated by the standard quadratic potential. However, we find that the number density and the formation rates of halos change by about 13–22% for halo masses ranging over 10^4 – $10^{14} M_{\odot}$, for potential parameters that lie within $2\text{-}\sigma$ around the best fit values arrived at from the aforesaid joint constraints. We briefly discuss the implications of our results.

*Current address: Asia Pacific Center for Theoretical Physics, Pohang, Gyeongbuk 790-784, Korea.

E-mail: dhiraj@apctp.org

Contents

1	Introduction	2
2	Primordial spectra with features	4
2.1	Essentials	4
2.2	Models of interest	5
2.3	Comparison with the WMAP and the SDSS data	6
3	From the primordial spectrum to the formation rate of halos	8
3.1	The matter power spectrum	8
3.2	Mass functions and the halo formation rates	9
4	Details of the numerical methods	10
5	Results	11
5.1	Joint constraints from the WMAP and the SDSS data	11
5.2	Effects of features on the number density and the formation rate of halos . .	12
6	Discussion	14

1 Introduction

Eversince its original proposal more than three decades ago, inflation has continued to be the most efficient scenario to overcome the horizon and the flatness problems associated with the conventional, hot big bang model. Additionally, inflation also provides an efficient mechanism for sowing the seeds of the density perturbations in the early universe [1, 2]. Over the last few years, observations of the Cosmic Microwave Background (CMB) by missions such as the Wilkinson’s Microwave Anisotropy Probe (WMAP) [3, 4] and the Atacama Cosmology Telescope (ACT) [5] have provided us with observational bounds on the parameters that describe the power spectra of the primordial perturbations. Currently, apart from the strong constraints on the primordial scalar amplitude and the spectral index, there also exists an upper bound on the tensor-to-scalar ratio. Clearly, the primordial power spectra generated by inflation must be consistent with these observational constraints.

The simplest mechanism to achieve inflation consists of a canonical scalar field (referred to as the inflaton) which rolls down slowly towards the minima of its potential. The perturbations originating from such a scalar field produces an almost scale independent power spectrum [1, 2]. Such a primordial spectrum, along with a suitable choice of parameters to describe the background Λ CDM model, is found to lead to a CMB angular power spectrum which fits the available observational data quite well. In fact, despite the constantly improving bounds, one finds that there exist many inflationary models that remain consistent with the observations.

However, there exist a few points (notably near the multipoles of $\ell = 2, 22$ and 40) in the WMAP data [3, 4], which lie outside the cosmic variance associated with the best fit theoretical curve corresponding to the CMB angular power spectra generated by slow

roll inflation. Though such outliers are few in number, demanding a better fit to these data points can, obviously, lead to a more favored model of inflation. Several attempts have been made to construct inflationary potentials that lead to wiggles in the primordial power spectrum (which, in turn, cause corresponding oscillations in the CMB angular power spectrum), thereby resulting in an improved fit to the data when compared to the featureless power spectra produced by slow roll inflation [6, 7, 8, 9]. The wiggles can be generated if the inflaton goes through a step or a bump in the potential. The presence of a step or a bump leads to a period of fast roll, which then leaves its imprints on the slow roll parameters and the power spectrum [10, 11]. Apart from constructing specific models that are more favored by the data, there has also been a few efforts towards a model independent reconstruction of the primordial scalar power spectrum from the observed CMB angular power spectrum [12]. Importantly, such reconstructions too seem to support the presence of features in the primordial power spectrum. Although the reconstruction efforts suggest that the features in the scalar power spectrum are typically localized over certain scales, it has been found that, oscillatory potentials which generate features on all scales also provide a much better fit to the CMB data than the nearly scale invariant power spectrum [13, 14, 15]. It may be worth mentioning here that inflationary models leading to features also gain importance due to the fact that they can generate large levels of non-Gaussianity as is possibly indicated by the WMAP data (in this context, see, for example, Refs. [16, 17] and the references therein).

Evidently, any significant change in the primordial power spectrum will correspondingly modify the matter power spectrum evaluated today. Hence, the features in the scalar perturbation spectrum that we mentioned above will affect the matter power spectrum which, in turn, will leave its signatures on the formation rates of the dark matter halos. The effects of steps or oscillations in the inflaton potential on the predicted number of halos was recently investigated based on the perturbation spectrum evaluated using the slow roll approximation [18]. However, the slow roll parameters can often turn large in such inflationary potentials and, as a result, the power spectrum evaluated in the slow roll approximation can differ considerably from the actual power spectrum. Moreover, with the ever increasing quality of the large scale structure observations, in particular, the halo power spectrum constructed using the Luminous Red Galaxies (LRG) from the seventh data release (DR7) of the Sloan Digital Sky Survey (SDSS) [19, 20], it would be a worthwhile exercise to actually compare the models with the available data to arrive at additional constraints (i.e. apart from those obtained from the CMB data) on the primordial features.

In this paper, we utilize a recently developed and accurate Fortran 90 code to *exactly* evaluate the inflationary perturbation spectrum, and thereby the corresponding matter power spectrum and the number of halos formed. We compute the number densities and the formation rates of halos in a couple of inflationary models that are known to lead to certain features in the power spectrum and also an improved fit to the CMB data. Our goal will be to estimate the maximum possible change in the number density and the formation rate of halos in these models, when compared with, say, inflation driven by the simplest quadratic potential. In order to arrive at the parameter space of interest, we shall compare the models with the CMB as well as the large scale structure data. Specifically, we shall make use of the WMAP seven year (WMAP-7) data [4] and the LRG halo power spectrum data from SDSS DR7 [20]. We find that the power spectra with features corresponding to the best

fit values of the inflationary parameters do not typically lead to substantial deviations in the formation rates of halos. However, we find that, in certain models that we consider, the potential parameters that lie within $2\text{-}\sigma$ of the best fit values obtained from the joint constraints of the WMAP and the SDSS data can lead to a 13–22% change in the number of halos formed for halo masses ranging over $10^4\text{--}10^{14} M_\odot$.

This paper is organized as follows. In the following section, we shall quickly describe the inflationary potentials of interest, which lead to specific features in the primordial scalar power spectrum. We shall also outline the method that we adopt to compare the models with the data. In Section 3, we shall outline the formalism to arrive at the matter power spectra and the halo formation rates from the inflationary power spectra. In Section 4, we shall provide a few essential details concerning the numerical procedures that we follow. We shall discuss the results in Section 5, and we shall close with a few concluding remarks regarding the wider implications of our results in Section 6.

Note that we shall assume the background cosmological model to be the standard, spatially flat, Λ CDM model.

2 Primordial spectra with features

In this section, we shall quickly sketch a few essential points concerning the scalar power spectrum generated during inflation. We shall also discuss the inflationary models of our interest and the scalar power spectra produced by them. Further, we shall outline the methods that we adopt to compare the models with the data.

2.1 Essentials

We shall focus on the simplest case of inflation driven by the canonical scalar field, say, ϕ . In a spatially flat Friedmann universe, given a potential $V(\phi)$, the scalar field satisfies the differential equation

$$\ddot{\phi} + 3H\dot{\phi} + V_\phi = 0, \quad (1)$$

where the overdot represents differentiation with respect to the cosmic time, $H = \dot{a}/a$ is the Hubble parameter, with a being the scale factor, while $V_\phi = dV/d\phi$. The evolution of the scalar field is usually characterized by a hierarchy of the so-called slow roll parameters. The first slow roll parameter is set to be $\epsilon_1 = -\dot{H}/H^2$, and the higher order slow roll parameters are defined in terms of the first as follows: $\epsilon_{i+1} = d \ln \epsilon_i / dN$, where $i \geq 1$ and N denotes the number of e-folds.

The scalar perturbations induced by the quantum fluctuations of the inflaton can be described by the curvature perturbation, say, \mathcal{R} , whose Fourier modes satisfy the following differential equation:

$$\mathcal{R}_k'' + 2\frac{z'}{z}\mathcal{R}_k' + k^2\mathcal{R}_k = 0, \quad (2)$$

where the overprime denotes differentiation with respect to the conformal time coordinate, and $z = a\dot{\phi}/H$. Upon solving this differential equation with suitable initial conditions for modes of cosmological interest, one arrives at the scalar power spectrum (see Section 4 for

the necessary details), defined as

$$\mathcal{P}_s(k) = \frac{k^3}{2\pi^2} |\mathcal{R}_k|^2, \quad (3)$$

with \mathcal{R}_k being evaluated at sufficiently late times. Smooth potentials, in general, permit slowly rolling fields (i.e. wherein the parameters ϵ_i are much smaller than unity), and such backgrounds generate nearly scale invariant power spectra. For instance, the archetypical quadratic potential, viz. $V(\phi) = m^2 \phi^2/2$, leads to the required COBE amplitude (for a suitable value of m) and an almost scale invariant spectrum with a scalar spectral index of $n_s \simeq 0.97$, in strong conformity with the recent CMB data [3, 4].

2.2 Models of interest

In contrast to smooth potentials, potentials that contain either non-trivial forms or sharp changes in their slopes lead to deviations from slow roll. Departures from slow roll affect the amplitude of the modes that leave the Hubble radius during this period resulting in specific features in the inflationary scalar power spectrum, with the shape being determined by the type of deviation from slow roll (in this context, see, for instance, Ref. [21]). Interestingly, certain features in the scalar power spectrum are known to allow an improved fit to the CMB data than the conventional nearly scale invariant spectrum, as is generated by slow roll inflation [6, 7, 8, 9, 13, 14, 15].

In this work, we shall consider two types of inflationary models that have been shown to fit the data better than the power law primordial spectrum. The first type of model that we shall consider contains a step, which is typically introduced in the conventional quadratic potential at a certain location, say, ϕ_0 , as follows [6, 9]:

$$V(\phi) = \frac{1}{2} m^2 \phi^2 \left[1 + \alpha \tanh \left(\frac{\phi - \phi_0}{\Delta\phi} \right) \right]. \quad (4)$$

Evidently, α and $\Delta\phi$ denote the strength and the width of the step, respectively. The field experiences a short period of fast roll as it crosses ϕ_0 , leading to a brief burst of oscillations in the scalar power spectrum. A Markov Chain Monte Carlo (MCMC) sampling of the parameter space of the above potential points to the fact that the presence of the step aids in fitting the outliers in the WMAP data near the multipoles of $\ell = 22$ and 40. In fact, at the expense of the three additional parameters, viz. ϕ_0 , α and $\Delta\phi$, the model results in an improvement in the effective least squares parameter χ_{eff}^2 by about 9, when compared with the quadratic potential without the step. In Figure 1, we have plotted the behavior of the first two slow roll parameters in the model.

Over the last few years, two types of oscillatory inflationary potentials have drawn a considerable amount attention [13, 14, 15, 17]. The first of these consists of the above-mentioned quadratic potential that is modulated by sinusoidal oscillations as follows:

$$V(\phi) = \frac{1}{2} m^2 \phi^2 \left[1 + \alpha \sin \left(\frac{\phi}{\beta} + \delta \right) \right]. \quad (5)$$

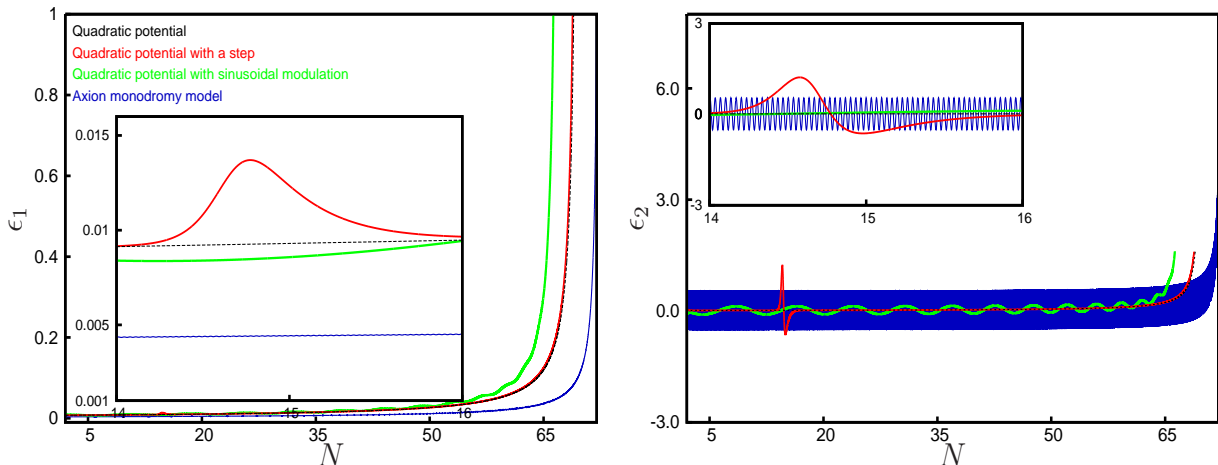


Figure 1: Evolution of the first two slow roll parameters ϵ_1 and ϵ_2 have been plotted as a function of the number of e-folds N for the quadratic potential without and with the step (the black and the red curves, respectively), the quadratic potential superimposed by sinusoidal modulations (the green curve) and the axion monodromy model (the blue curve). The curves have been plotted for potential parameters that lead to the best fit to the recent WMAP and SDSS data. In the quadratic potential without the step, as is well known, the field continues to roll slowly until the end of inflation, whereas, when the step is introduced, it briefly deviates from slow roll around the time the field crosses the step. In the case of the potentials with oscillations, for the best fit values, the axion monodromy model leads to strong departures from slow roll, with ϵ_2 turning large repeatedly, right till the termination of inflation. The insets provide a closer view of the behavior of the slow roll parameters over a smaller range of e-folds.

The second is the so-called axion monodromy model that has its motivations in string theory, and is described by the potential

$$V(\phi) = \lambda \left[\phi + \alpha M_{\text{Pl}} \cos \left(\frac{\phi}{\beta} + \delta \right) \right]. \quad (6)$$

In both these cases, the slow roll parameters oscillate and, in fact, continue to exhibit such a behavior until the termination of inflation (cf. Figure 1). All modes of interest are affected by these oscillations, which leave a repeated pattern that extends over all scales in the power spectrum. We shall illustrate the power spectra resulting in these models later in Section 5 (see Figure 3), wherein we shall present the results of our analysis. We would like to mention here that recent analysis indicate that such power spectra lead to an improved fit to the WMAP as well as the small scale ACT data. In the case of the quadratic potential modulated by sinusoidal oscillations, one finds that the least squares parameter χ_{eff}^2 reduces by about unity, whereas the monodromy model is found to lead to a much better fit to the data with an improvement in χ_{eff}^2 of up to 13, when compared with a more conventional, nearly scale invariant spectrum [14, 15].

2.3 Comparison with the WMAP and the SDSS data

We shall compare the models with the CMB as well as the large scale structure data. We have worked with the WMAP-7 data [4] and the halo power spectrum data arrived at from the LRG in SDSS DR7 [20]. We have made use of the large scale structure data to ensure

that the parameter values we eventually work with to obtain the formation rate of the halos are consistent with the observed matter power spectrum.

We have made use of the publicly available codes, viz. the cosmological Boltzmann code CAMB [22, 23] and the Monte Carlo code COSMOMC [24, 25], to compute the CMB angular and the matter power spectra, and compare them with the data, respectively. As we had mentioned, we shall assume the background model to be the spatially flat Λ CDM and we shall work with the priors on the background parameters as listed in Table 1.

Background parameter	Lower limit	Upper limit
$\Omega_b h^2$	0.005	0.1
$\Omega_c h^2$	0.01	0.99
θ	0.5	10.0
τ	0.01	0.8

Table 1: The priors on the four parameters that describe the background, spatially flat, Λ CDM model. The quantities $\Omega_b h^2$ and $\Omega_c h^2$ describe the baryon and CDM densities (with h being related to the Hubble parameter), θ is the ratio of the sound horizon to the angular diameter distance at decoupling, while τ is the optical depth to reionization. We should mention that we keep the same priors on the background parameters for all the COSMOMC analysis in this paper.

We should note here that the step model (4), the quadratic potential with the sinusoidal modulation (5) and the axion monodromy model (6), all require four parameters to describe the potential completely. As far as the priors on these parameters are concerned, for the case of the quadratic potential with the step, we have worked with the same priors as we had worked with before [9]. In the case of the quadratic potential with superimposed sinusoidal modulations and the axion monodromy model, for the primary parameters m and λ , we work with the same priors that we had considered in a recent analysis wherein we had compared the models with the CMB data [15]. However, while comparing with the WMAP as well as the SDSS data, we have widened the priors of the parameters α and β for both the oscillatory potentials as listed in Table 2. We should add that we have allowed the phase parameter δ to vary from $-\pi$ to π as before.

Model	Potential parameter	Lower limit	Upper limit
Quadratic potential with sinusoidal modulation	α	0	2×10^{-3}
	$\ln(\beta/M_{\text{Pl}})$	-3.9	0
Axion monodromy model	α	0	2×10^{-4}
	$\ln(\beta/M_{\text{Pl}})$	-8	0

Table 2: The widened priors on the parameters α and β of the potentials (5) and (6). Note that the priors are considerably wider than the limits in our recent analysis [15]. Also, we have also worked with the logarithmic value of β in order to cover a larger range with a uniform weightage.

The motivations for these choice of priors are two fold. Firstly, while determining the priors on the parameters m and λ , we have ensured that the resulting inflationary power

spectra do not differ considerably from the nearly scale invariant spectrum for the faster convergence of the Markov Chains. Secondly, we have chosen the priors on α and β such that the scalar field does not get trapped by the oscillations in the potential.

We should mention that, unlike in our earlier efforts [9, 15], we have not taken the effects of the tensor perturbations into account, as the corresponding effects are negligible. Moreover, in the case of potentials with oscillations, which lead to fine features in the inflationary scalar power spectrum, we actually need to modify CAMB in order to ensure that the CMB angular power spectrum is evaluated at every multipole and compare them with the data [14, 15, 26]. But, we have not implemented this point here since we are only interested in the marginalized probabilities of the potential parameters. These probabilities shall indicate the extent to which deviations from a nearly scale invariant spectrum is allowed by the data, and the corresponding effects on the formation of dark matter halos. We should point out that we have not taken into account the non-linear effects on the matter power spectrum [27], but have included the SZ effect and the effects due to gravitational lensing in our analysis. Finally, we shall set the Gelman and Rubin parameter $|R - 1|$ to be 0.03 for convergence in all the cases.

3 From the primordial spectrum to the formation rate of halos

In this section, we shall quickly outline the standard formalism to arrive at the formation rate of halos from the primordial power spectrum.

3.1 The matter power spectrum

Given a primordial power spectrum, say, $\mathcal{P}_s(k)$ [cf. Eq. (3)], the matter power spectrum at the redshift z is usually written as (see, for example, Refs. [28, 29])

$$P_M(k, z) = \left(\frac{2}{5\Omega_m}\right)^2 \left(\frac{k}{a_0 H_0}\right)^4 \left(\frac{2\pi^2}{k^3}\right) \mathcal{P}_s(k) T^2(k) D_+^2(z), \quad (7)$$

a quantity that can be conveniently expressed in units of Mpc^3 for the modes of cosmological interest. In the above expression, $T(k)$ is the CDM transfer function, the quantity $D_+(z)$ denotes the linear growth factor of the total matter perturbation, Ω_m is the non-relativistic density parameter, while a_0 and H_0 denote the scale factor and the Hubble parameter today.

If we define $D_+(a) = g(a)/a$, then, one finds that, in the spatially flat Λ CDM model, the quantity g satisfies the differential equation [3, 30]

$$\frac{d^2 g}{d \ln a^2} + \frac{1}{2} [5 + 3\Omega_\Lambda(a)] \frac{dg}{d \ln a} + 3\Omega_{\text{eff}}(a) g = 0, \quad (8)$$

where $\Omega_{\text{eff}}(a) = \Omega_\Lambda H_0^2/H^2$, with Ω_Λ denoting the dimensionless density parameter associated with the cosmological constant today. In this work, we shall solve the above differential equation with suitable initial conditions to obtain the growth factor $D_+(a)$. Utilizing CAMB [22, 23] to determine the corresponding transfer function $T(k)$ and, upon using the

primordial spectrum obtained numerically in the inflationary model of interest, we shall eventually arrive at the matter power spectrum (see Section 4 on numerical methods for further details).

3.2 Mass functions and the halo formation rates

To arrive at the formation rate of dark matter halos, we shall first require the number density of collapsed halos with mass in the range of M and $M + \delta M$ in a comoving volume element. This number density, say, $n(M)$, is defined in terms of the root mean square fluctuation in mass σ through the so-called mass function $f(\sigma)$ as follows [31]:

$$\frac{dn}{d \ln M} = -\frac{2 \rho_m}{M} \left(\frac{d \ln \sigma(R)}{d \ln M} \right) f(\sigma), \quad (9)$$

where ρ_m is the mean density of non-relativistic matter in the universe. Following the convention (see, for example, Ref. [28]), we shall define the root mean square fluctuation in mass at the scale R to be

$$\sigma^2(R) = \int_0^\infty d \ln k \mathcal{P}_M(k) \widetilde{W}^2(k, R), \quad (10)$$

where $\mathcal{P}_M(k) \equiv k^3 P_M(k)/(2\pi^2)$ denotes the *dimensionless* matter power spectrum, while $\widetilde{W}(k, R)$ is the Fourier transform of the window function $W(x, R)$ that is introduced to smooth out the density perturbation. We shall work with the commonly used spherical top hat window function, whose Fourier transform is given by

$$\widetilde{W}(k, R) = \widetilde{W}(k R) = 3 \frac{\sin(k R) - k R \cos(k R)}{(k R)^3}, \quad (11)$$

corresponding to the volume $V(R) = 4\pi R^3/3$. Note that the halo mass M within the window of radius R is given by $M(R) = \rho_m V(R)$.

We shall make use of the Sheth-Tormen mass function to evaluate the number density of halos [32]. In contrast to the more conventional Press-Schechter mass function [33], it has been found that the Sheth-Tormen mass function fits the data from the N -body simulations better. Actually, the Sheth-Tormen mass function is a generalization of the original Press-Schechter formalism for spherical collapse to the case of ellipsoidal collapse. The Sheth-Tormen mass function is defined in terms of two additional parameters b and p (when compared to the Press-Schechter case) as follows:

$$f(\sigma) = A \sqrt{\frac{b\nu}{2\pi}} [1 + (b\nu)^{-p}] \exp - (b\nu/2), \quad (12)$$

where $\nu = (\delta_c/\sigma)^2$, with $\delta_c = 1.686$ being the threshold linear overdensity for collapse. The Press-Schechter mass function corresponds to $A = 1/2$, $b = 1$ and $p = 0$. However, upon comparing with the N -body simulation data, the best fit values for b and p are found out to be 0.707 and 0.3, respectively. The value of A can then be arrived at from the normalization condition on $f(\nu)$, viz. that the integral of $f(\nu)/\nu$ over all ν is unity, which leads to $A = 0.3222$.

The number density of halos associated with the above Sheth-Tormen mass function is then given by

$$\frac{dn}{d \ln M} = -\frac{A \rho_m}{M} \sqrt{\frac{2b\nu}{\pi}} [1 + (b\nu)^{-p}] \left(\frac{d \ln \sigma}{d \ln M} \right) \exp - (b\nu/2). \quad (13)$$

The corresponding formation rates of the halos can be easily obtained to be [34]

$$R(M, z) = -\frac{dD_+(z)}{dz} \frac{dz}{dt} \frac{1}{D_+(z)} \left[\frac{2p}{1 + (b\nu)^{-p}} - b\nu \right] \frac{dn}{dM}. \quad (14)$$

Note that the quantity dD_+/dz proves to be negative, since the growth factor decreases as the redshift increases. As a result, it is known that the above formation rate of halos can become negative for some mass scales (i.e. when $2p/[1 + (b\nu)^{-p}] > b\nu$), which in practice can not occur. Therefore, to avoid this issue and simultaneously illustrate the effects of features, we shall only plot the ratio of the formation rates in the inflationary models leading to features and the conventional, smooth, quadratic potential.

4 Details of the numerical methods

The slow roll approximation allows the background as well as the perturbations to be evaluated analytically during inflation. As we pointed out before, in the earlier work [18], it was the slow roll approximation that was made use of in order to arrive at the inflationary perturbation spectrum $\mathcal{P}_s(k)$. However, we find that, in the inflationary models of interest, the slow roll parameters turn sufficiently large (cf. Figure 1) implying a breakdown of the slow roll approximation. As a result, we resort to numerical methods to compute the primordial perturbation spectrum. In fact, we utilize a Fortran 90 code that has been recently developed by us, which makes use of a Bulirsch-Stoer algorithm along with an adaptive step size control routine [35] to accurately and efficiently solve the equations governing the background and the perturbations, in order to arrive at the inflationary scalar power spectrum (see Refs. [9, 15] for further details in this regard).

Having computed the primordial power spectrum, we arrive at the matter power spectrum using the transfer function and the growth factor. As we had remarked earlier, we obtain the transfer function from CAMB, and we evaluate the growth factor by solving the differential equation (8). It should be mentioned here that the initial conditions are chosen such that g is a constant and equal to unity in the early matter dominated epoch, i.e. at a sufficiently high redshift of, say, $z \simeq 30$ [3, 36].

After having obtained the matter power spectrum, we calculate the variance $\sigma(R)$ using equation (10). The integral can be evaluated numerically with the simplest of algorithms, provided the power spectrum proves to be smooth and devoid of any features. In contrast, when these exist features such as repeated oscillations, certain care is required, and we have made use of an adaptive integration routine to compute the integral involved [37]. We have carried out integral from a suitably small mode (such as $k = 10^{-5} \text{Mpc}^{-1}$) up to a mode where the window function cuts off the integrand. Finally, we obtain the quantity $d \ln \sigma / d \ln M$ by numerical differentiation. We should stress here that, keeping in mind the presence of

oscillations in the power spectra, we have computed σ and $d \ln \sigma / d \ln M$ with care and high accuracy. We should also add that we have cross checked our result by fitting the numerical values of $\sigma(R)$ to the Chebyshev polynomials and calculating the corresponding derivative from the polynomial (in this context, see Ref. [36]).

5 Results

In this section, we shall present the results of our comparison of the models of our interest with the CMB and the large scale structure data. We shall also discuss the effects of primordial spectra with features on the formation of halos.

5.1 Joint constraints from the WMAP and the SDSS data

In Table 3 below, we have tabulated the best fit values of the background and the potential parameters obtained from the MCMC analysis using the WMAP-7 and the SDSS LRG DR7 data. We have also listed the effective least squared parameter χ_{eff}^2 in each of the cases. For the case of the quadratic potential with and without the step, we have arrived at results similar to what we have obtained in an earlier work [9]. Also, as one would expect, we find that the background parameters are better constrained with the inclusion of the additional SDSS data [38, 39]. Moreover, it is obvious from Table 3 that the axion monodromy model does not lead to the same extent of improvement in the fit as has been obtained before (in this context, see Refs. [14, 15]). This arises due to the fact that, unlike in the earlier analysis, we have not evaluated the CMB angular power at each multipole, but have worked with the inbuilt effective sampling and interpolation routine in CAMB. However, we should stress that this does not affect our conclusions since our focus here lies on the maximum change in the formation of halos. Therefore, we are more interested in the allowed regions of the parameter space of rather in arriving at the precise best fit point. Also, importantly, as we shall discuss in the following subsection, for violent oscillations in the primordial power spectrum (when one requires computing the CMB angular power spectrum at each multipole explicitly and accurately), the percentage change in the number density of halos proves to be negligible in the observable mass bins.

In Figure 2, we have illustrated the one dimensional likelihood on the parameter ϕ_0 in the case of the quadratic potential with a step, and it is clear that the location of the step is highly constrained by data. The step affects the number density of halos over only highly localized mass scales. We have also plotted the marginalized two dimensional constraints on the parameters α and β for the cases of the two oscillatory potentials. It is noteworthy that the constraints are strikingly similar. In fact, the roughly triangular shape of the contours can also be understood. As the parameter β decreases, the resulting oscillations in the potential and, therefore, in the inflationary perturbation spectrum turn too frequent, and the data constrains the amplitude α to a smaller region.

In Figure 3, we have plotted the best fit scalar power spectrum for quadratic potential with and without the step and the two oscillatory potentials. Further below, in Figure 4, we have plotted the matter power spectrum $P_M(k)$ evaluated *today* corresponding to the different inflationary power spectra in the previous figure. In the inset of the figure, we have

Model	Quadratic	Quadratic + step	Quadratic + sine	Axion monodromy
$\Omega_b h^2$	0.0222	0.0221	0.0216	0.0225
$\Omega_c h^2$	0.1162	0.1159	0.1168	0.1154
θ	1.038	1.039	1.036	1.039
τ	0.0824	0.0875	0.0836	0.0856
$\ln(10^{10} A)$	-0.6545	-0.6406	-0.6448	0.9649
α	-	1.61×10^{-3}	6.35×10^{-5}	4.4×10^{-5}
ϕ_0/M_{Pl}	-	14.664	-	-
$\Delta\phi/M_{\text{Pl}}$	-	3.22×10^{-3}	-	-
$\ln(\beta/M_{\text{Pl}})$	-	-	-2.576	-7.61
δ	-	-	2.208	-1.178
χ_{eff}^2	7515.57	7507.3	7515.12	7509.56

Table 3: The best fit values for the background and the potential parameters for the different models of interest obtained from the MCMC analysis using the WMAP-7 and the SDSS LRG DR7 data. We should mention here that the parameter A denotes λ/M_{Pl}^3 in the case of axion monodromy model and m^2/M_{Pl}^2 in rest of the cases. As we have discussed before, the quadratic potential with the step improves the fit to the outliers in the CMB data around the multipoles of $\ell = 22$ and 40. Moreover, as we have pointed out, while the superimposed sinusoidal modulation to the quadratic potential does not provide a better fit to the data when compared to the quadratic potential, the axion monodromy model improves the fit to a good extent. However, note that, the monodromy model does not improve the fit to the data to the same extent that as has been arrived at recently [14, 15]. As we have pointed out in the text, this arises due to the limited sampling and interpolation by CAMB over the multipoles of interest.

highlighted the baryon acoustic oscillations and the halo power spectrum data from SDSS LRG DR7. We should add here that the theoretical best fit curves are unable to fit the data well after $k \sim 0.1 h \text{ Mpc}^{-1}$ due to the fact that we have not taken the non-linear effects into account in arriving at the matter power spectrum.

5.2 Effects of features on the number density and the formation rate of halos

In this subsection, we shall discuss the effects of the features on the number density and the formation rates of halos in the different inflationary models of our interest. In order to highlight the effects purely due to the primordial features, we have frozen the values of the background cosmological parameters, viz. Ω_m , Ω_Λ , H_0 and the dimensionless baryon density parameter Ω_b at the values arrived at upon comparing the smooth quadratic potential with the WMAP and SDSS data, as listed in Table 3. But, we have made use of the best fit values for the potential parameters to compute the inflationary scalar power spectrum and from thereon the matter power spectrum and the number density of halos. In Figure 5, we have plotted the percentage of change in the formation rate of halos in the Press-Schechter formalism and the number density of halos in the Sheth-Tormen formalism for different models with respect to the quadratic potential. In the case of the model with the step, the change in the number density due to the step (corresponding to parameter values within $2\text{-}\sigma$ around the best fit values) occurs at very high mass halos ($\sim 10^{17} M_\odot$) and hence lies outside

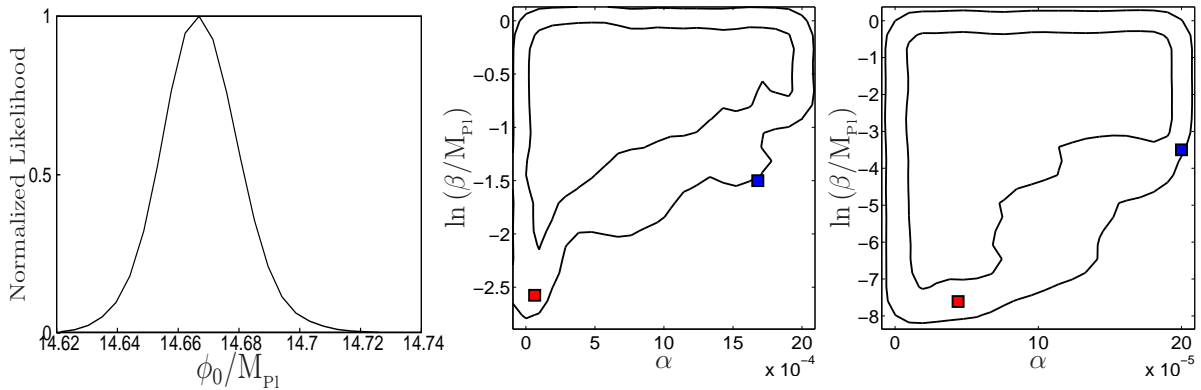


Figure 2: The one dimensional likelihood on the parameter ϕ_0 in the case of the quadratic potential with a step (on the left) and the two dimensional constraints on the parameters α and β in the cases of the quadratic potential with sinusoidal modulations (in the middle) and the axion monodromy model (on the right). Note that the location of the step ϕ_0 is well constrained. The inner and the outer curves (in the figure in the middle and the one on the right) correspond to the $1\text{-}\sigma$ and the $2\text{-}\sigma$ confidence contours. The red points appearing in the two plots on the right correspond to the best fit values of α and β , while the blue points indicate a sample point in the parameter space at and around which the maximum deviation in number density of halos occurs, when compared to the more conventional quadratic model (in this context, see Figure 5). We should highlight here the fact that, in the cases of both the inflationary models with oscillations in the potential (i.e. the chaotic model with sinusoidal modulation as well as the axion monodromy model), the best fit values of α and $\ln \beta$ lie outside the $1\text{-}\sigma$ marginalized contours. We find that this occurs because of the reason that the marginalized one-dimensional probability distributions of these parameters are highly skewed. This in turn indicates that a good improvement in the fit occurs in a small region of the parameter space with a low marginalized probability.

our region of interest. Due to this reason, we have only presented the results in the case of the models with oscillatory terms in the potential.

In order to arrive at the maximum possible change in the number density of halos when compared to the conventional nearly scale invariant primordial spectrum, for the models with oscillations in the potential, we have chosen values for the parameters α and β that they lie within (actually, *at*) $2\text{-}\sigma$ from the best fit values. We have chosen the parameters in such a way that they create the largest deviation from the nearly scale invariant power spectra that are allowed by the CMB and observations of the large scale structure. In Figure 5, apart from the results for the best fit values, we have plotted the number density and the formation rates of halos for the cases wherein $[\alpha, \ln(\beta/M_{\text{Pl}})]$ is set to $(1.7 \times 10^{-3}, -1.5)$ and $(2 \times 10^{-4}, -3.5)$ (as indicated by the blue points in Figure 2) for the quadratic potential with sinusoidal modulations and the axion monodromy model, respectively. In arriving at these plots, we have fixed the parameters m and λ at their best fit values as shown in the Table 3, since these parameters do not play a role in altering the features in the spectrum. We have also chosen the value of δ to be the best fit value for both the models. It is evident from the figure that, for the best fit values of the parameters, the change in the number density is completely negligible ($\sim 2\%$). However, we find that, for the case of the quadratic potential with sinusoidal modulation, the numbers can change by as much as 22% for values of the potential parameters α and β that lie within $2\text{-}\sigma$. It should also be highlighted that the monodromy model does not seem to lead to the same extent of change in the number

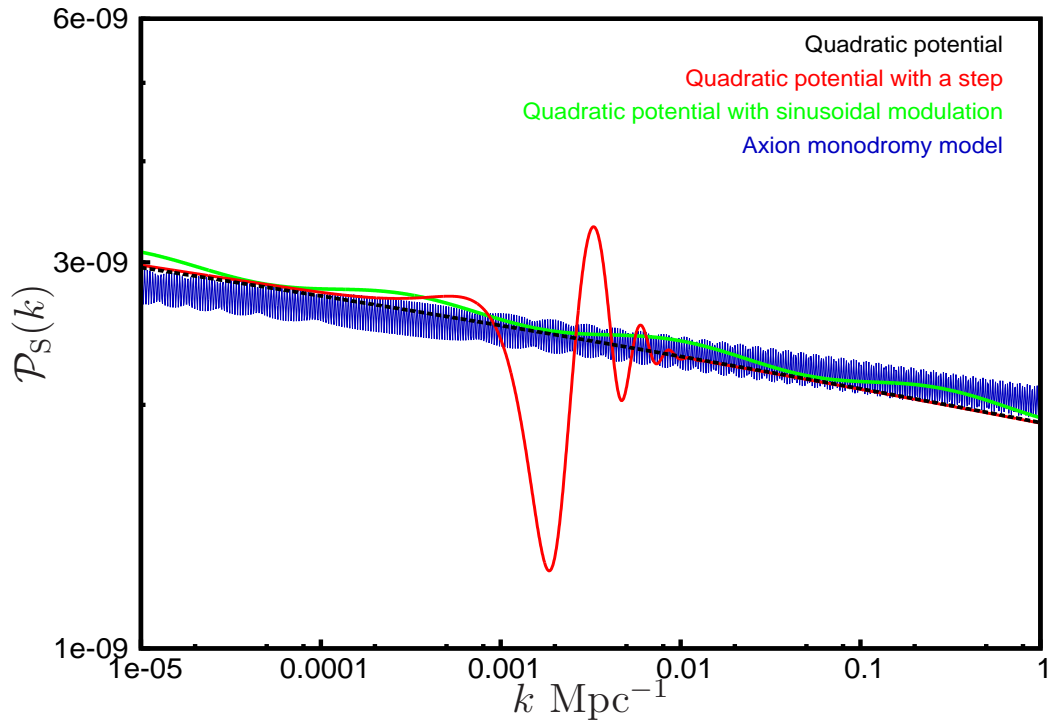


Figure 3: The scalar power spectra that arise in the four inflationary models of our interest. These spectra correspond to the best fit values for which we had plotted the evolution of the first two slow roll parameters in Figure 1. Note that, we have worked with the same choice of colors to represent the results from the different models as in the earlier figure. We should emphasize that, while the step model leads to features that are localized, the potentials with oscillatory terms lead to modulations in the scalar power spectrum that extend over a wide range of scales.

density and the rate of formation of halos, despite the fact that it produces fine oscillations in the primordial as well as the linear matter power spectra (cf. Figures 3 and 4). Actually, while the *unbinned* number density does indicate a 5–15% change, we find that, the change proves to be smaller when we bin the numbers in logarithmic mass bins, i.e. $\Delta \log_{10}(M/M_{\odot})$, of 0.2. Evidently, binning seems to average out the rapid oscillations, resulting in a smaller extent of change in the numbers.

6 Discussion

In this work, we have investigated the effects of primordial features on the matter power spectrum as well as the number of halos formed and their rate of formation. Similar work in this context [18] had suggested that a small change in the parameters describing the inflaton potential would lead to a drastic change in the number of halos formed. The earlier work was based on the inflationary perturbation spectrum that was arrived at based on the slow roll approximation. In contrast, we have carried a complete and accurate numerical analysis. Further, we have made use of the Sheth-Tormen mass function (instead of the older Press-Schechter one) which is known to fit the data from the N -body simulations better. We have

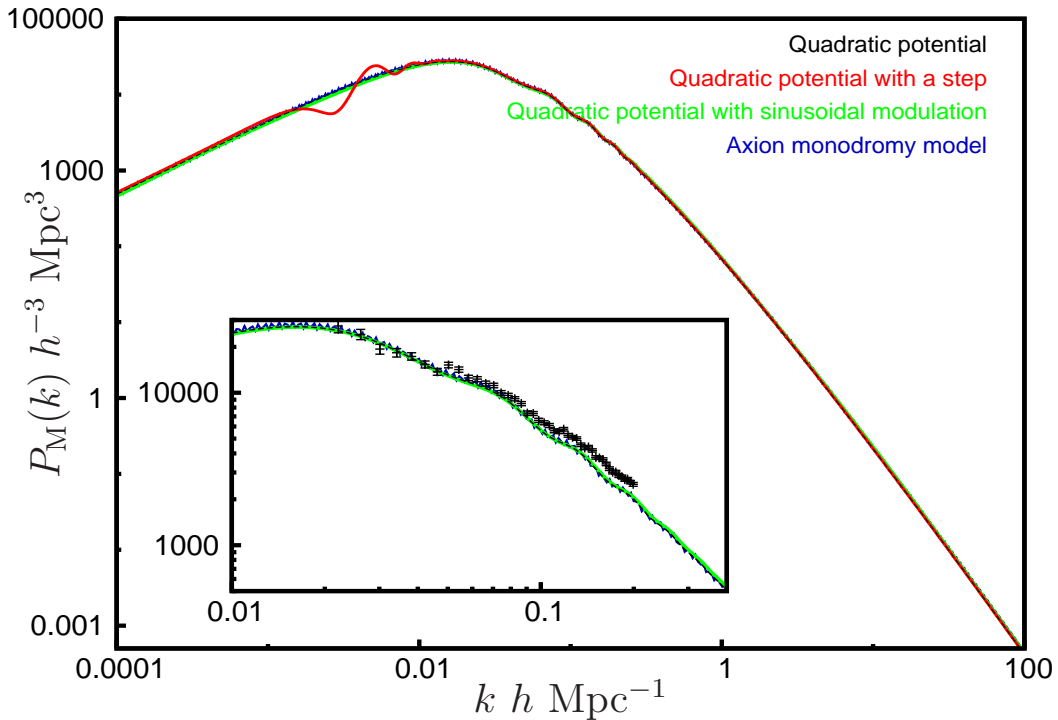


Figure 4: The best fit matter power spectrum $P_M(k)$ corresponding to the different inflationary scalar power spectra we had plotted in the previous figure. The inset highlights the imprints of the primordial features on the matter power spectrum in the domain where the baryon acoustic oscillations also play a role. The black dots with bars correspond to the power spectrum data from SDSS obtained upon combining main galaxies and the LRGs with error bars arrived at from the diagonal elements of the corresponding covariance matrix. It should be noted that, since we have plotted the linear power spectrum, without taking into account the non-linear effects, the theoretical best fit curves are unable to fit the data well for $k > 0.1 h \text{ Mpc}^{-1}$ (in this context, see Ref. [27]).

included the baryon acoustic oscillations in our analysis to have a more realistic comparison. Moreover, to arrive at the parameter space of interest, all the potentials considered in our work have been constrained by an MCMC analysis (using COSMOMC) against the WMAP-7 and SDSS LRG DR7 datasets. We find that, the best fit values for the potential parameters (with the background parameters kept fixed) lead to hardly any change in the number of halos formed when compared to the conventional quadratic potential that generates a nearly scale invariant primordial spectrum. However, partly consistent with the earlier result, we find that values for the potential parameters that lie within $2\text{-}\sigma$ of the best fit values indeed lead to a reasonable change in the number of halos formed and in their formation rates. For instance, we find that, with superimposed sinusoidal modulations, the quadratic potential leads to as much as a 13–22% change in the halo number density and the rate of formation. Needless to mention, the step of comparing the models against the data is crucial as this imposes real bounds on the extent of changes in the numbers involved. It is worthwhile to note that the inclusion of SDSS data reduces the maximum change in number density to about 10%, when compared to the case wherein one works with the parameters constrained by the WMAP data alone.

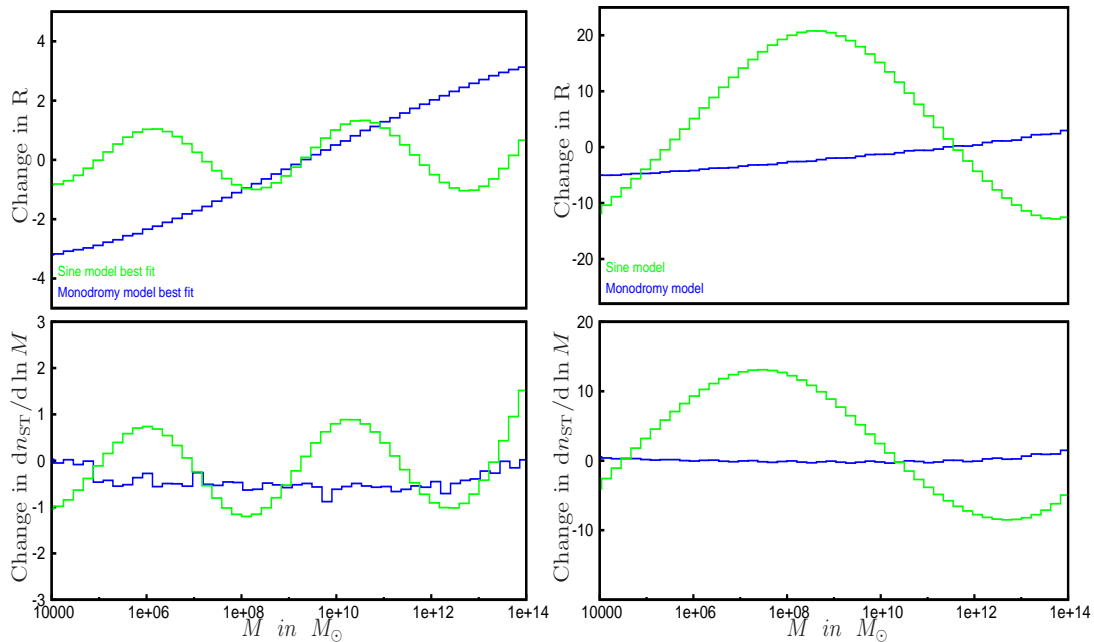


Figure 5: The percentage change in the formation rate of halos (in the Press-Schechter formalism, on top) and in their number density (in the Sheth-Tormen formalism, at the bottom) for the two inflationary models containing oscillatory terms, with respect to the more conventional quadratic potential. The figures on the left correspond to the best fit values (indicated by the red points in Figure 2), while those on the right correspond to values chosen within (in fact, *on*) the $2\text{-}\sigma$ confidence contours of the parameters α and β , determined from the joint constraints of the WMAP and SDSS data (indicated by the blue points in Figure 2). In order to highlight the effects due to the primordial features, we have frozen the background parameters at the best fit values arrived at when the primordial spectrum is determined by the quadratic potential. We have then worked with the best fit values for the potential parameters to arrive at the figures on the left. We have plotted the percentage change in logarithmic mass bins, i.e. $\Delta \log_{10}(M/M_{\odot})$, of 0.2. It is clear that the features corresponding to the best fit values do not lead to any substantial difference in either the number or the formation rates of the halos. However, note that the quadratic potential with superimposed sinusoidal oscillations leads to a 13% change in the number of halos formed when we choose to work with values of α and β that lie within the $2\text{-}\sigma$ contours.

We would like to close this paper with the following remarks. As we had pointed out before, while comparing with the SDSS data, we have not taken into account the non-linear effects on the matter power spectrum. It is for this reason that the theoretical curve had not fit the observational data well on small scales (cf. Figure 4). Clearly, a more complete analysis should involve modeling of the non-linear effects and their inclusion in evaluating the matter power spectrum [27]. For instance, it will be interesting to compare the results on the number of halos formed in numerical simulations, evolved from primordial spectra with features, with the small scale data.

Acknowledgments

The author wishes to thank Shiv Sethi and L. Sriramkumar for discussions as well as comments on the manuscript. Computational work for this study has been carried out using the cluster computing facilities at Harish-Chandra Research Institute, Allahabad, India (<http://cluster.hri.res.in/>).

References

- [1] E. W. Kolb and M. S. Turner, *The Early Universe* (Addison-Wesley, Redwood City, California, 1990); S. Dodelson, *Modern Cosmology* (Academic Press, San Diego, U.S.A., 2003); V. F. Mukhanov, *Physical Foundations of Cosmology* (Cambridge University Press, Cambridge, England, 2005); S. Weinberg, *Cosmology* (Oxford University Press, Oxford, England, 2008); R. Durrer, *The Cosmic Microwave Background* (Cambridge University Press, Cambridge, England, 2008); D. H. Lyth and A. R. Liddle, *The Primordial Density Perturbation* (Cambridge University Press, Cambridge, England, 2009); P. Peter, J-P. Uzan and J. Brujic, *Primordial Cosmology* (Oxford University Press, Oxford, England, 2009).
- [2] H. Kodama and M. Sasaki, *Prog. Theor. Phys. Suppl.* **78**, 1 (1984); V. F. Mukhanov, H. A. Feldman and R. H. Brandenberger, *Phys. Rep.* **215**, 203 (1992); J. E. Lidsey, A. Liddle, E. W. Kolb, E. J. Copeland, T. Barreiro and M. Abney, *Rev. Mod. Phys.* **69**, 373 (1997); D. H. Lyth and A. Riotto, *Phys. Rep.* **314**, 1 (1999); A. Riotto, [arXiv:hep-ph/0210162](https://arxiv.org/abs/hep-ph/0210162); J. Martin, [arXiv:hep-th/0406011](https://arxiv.org/abs/hep-th/0406011); B. Bassett, S. Tsujikawa and D. Wands, *Rev. Mod. Phys.* **78**, 537 (2006); W. H. Kinney, [arXiv:0902.1529](https://arxiv.org/abs/astro-ph.CO/0902.1529) [astro-ph.CO]; L. Sriramkumar, *Curr. Sci.* **97**, 868 (2009); D. Baumann, [arXiv:0907.5424](https://arxiv.org/abs/0907.5424)v1 [hep-th].
- [3] J. Dunkley *et al.*, *Astrophys. J. Suppl.* **180**, 306 (2009); E. Komatsu *et al.*, *Astrophys. J. Suppl.* **180**, 330 (2009).
- [4] D. Larson *et al.*, *Astrophys. J. Suppl.* **192**, 16 (2011); E. Komatsu *et al.*, *Astrophys. J. Suppl.* **192**, 18 (2011).
- [5] J. Dunkley *et al.*, *Astrophys. J.* **739**, 52 (2011).
- [6] J. A. Adams, B. Cresswell and R. Easther, *Phys. Rev. D* **64**, 123514 (2001); L. Covi, J. Hamann, A. Melchiorri, A. Slosar and I. Sorbera, *Phys. Rev. D* **74**, 083509 (2006); J. Hamann, L. Covi, A. Melchiorri and A. Slosar, *Phys. Rev. D* **76**, 023503 (2007); M. J. Mortonson, C. Dvorkin, H. V. Peiris and W. Hu, *Phys. Rev. D* **79**, 103519 (2009).
- [7] M. Joy, V. Sahni and A. A. Starobinsky, *Phys. Rev. D* **77**, 023514 (2008); M. Joy, A. Shafieloo, V. Sahni and A. A. Starobinsky, *JCAP* **0906**, 028 (2009).
- [8] R. K. Jain, P. Chingangbam, J.-O. Gong, L. Sriramkumar and T. Souradeep, *JCAP* **0901**, 009 (2009); R. K. Jain, P. Chingangbam, L. Sriramkumar and T. Souradeep, *Phys. Rev. D* **82**, 023509 (2010).

- [9] D. K. Hazra, M. Aich, R. K. Jain, L. Sriramkumar and T. Souradeep, JCAP **1010**, 008 (2010).
- [10] A. A. Starobinsky, Sov. Phys. JETP Lett. **55**, 489 (1992).
- [11] C. Dvorkin and W. Hu, Phys. Rev. D **81**, 023518 (2010); W. Hu, Phys. Rev. D **84**, 027303 (2011).
- [12] S. Hannestad, Phys. Rev. D **63**, 043009 (2001); S. L. Bridle, A. M. Lewis, J. Weller and G. Efstathiou, Mon. Not. Roy. Astron. Soc. **342**, L72 (2003); P. Mukherjee and Y. Wang, Astrophys. J. **599**, 1 (2003); S. Hannestad, JCAP **0404**, 002 (2004); A. Shafieloo and T. Souradeep, Phys. Rev. D **70**, 043523 (2004); D. Tocchini-Valentini, Y. Hoffman and J. Silk, Mon. Not. Roy. Astron. Soc. **367**, 1095 (2006); A. Shafieloo, T. Souradeep, P. Manimaran, P. K. Panigrahi and R. Rangarajan, Phys. Rev. D **75**, 123502 (2007); A. Shafieloo and T. Souradeep, Phys. Rev. D **78**, 023511 (2008); R. Nagata and J. Yokoyama, Phys. Rev. D **79**, 043010 (2009); G. Nicholson and C. R. Contaldi, JCAP **0907**, 011 (2009).
- [13] C. Pahud, M. Kamionkowski and A. R. Liddle, Phys. Rev. D **79**, 083503 (2009).
- [14] R. Flauger, L. McAllister, E. Pajer, A. Westphal and G. Xu, JCAP **1006**, 009 (2010).
- [15] M. Aich, D. K. Hazra, L. Sriramkumar and T. Souradeep, [arXiv:1106.2798v2](https://arxiv.org/abs/1106.2798) [astro-ph.CO].
- [16] J. Maldacena, JHEP **0305**, 013 (2003); D. Seery and J. E. Lidsey, JCAP **0506**, 003 (2005); X. Chen, Adv. Astron. **2010**, 638979 (2010).
- [17] X. Chen, R. Easther, E. A. Lim, JCAP **0804**, 010 (2008); R. Flauger and E. Pajer, JCAP **1101**, 017 (2011); F. Arroja, A. E. Romano and M. Sasaki, Phys. Rev. D **84**, 123503 (2011); J. Martin and L. Sriramkumar, JCAP **1201**, 008 (2012); D. K. Hazra, L. Sriramkumar and J. Martin, [arXiv:1201.0926v1](https://arxiv.org/abs/1201.0926) [astro-ph.CO]; F. Arroja and M. Sasaki, JCAP **1208**, 012 (2012).
- [18] L. F. S. Rodrigues and R. Opher, Phys. Rev. D **82**, 023501 (2010).
- [19] See, for instance, <http://www.sdss.org/>
- [20] K. Abazajian *et. al.* Astrophys. J. Suppl. **182**, 543-558 (2009)
- [21] R. K. Jain, P. Chingangbam and L. Sriramkumar, JCAP **10**, 003 (2007).
- [22] See, <http://camb.info/>.
- [23] A. Lewis, A. Challinor and A. Lasenby, Astrophys. J. **538**, 473 (2000).
- [24] See, <http://cosmologist.info/cosmomc/>.
- [25] A. Lewis and S. Bridle, Phys. Rev. D **66**, 103511 (2002).

- [26] Z. Huang, JCAP **1206**, 012 (2012).
- [27] R. E. Smith *et al.*, Mon. Not. Roy. Astron. Soc. **341**, 1311 (2003); M. Tegmark *et al.*, Phys. Rev. D **74**, 123507 (2006); W. J. Percival *et al.*, Astrophys. J. **657**, 645 (2007).
- [28] H. Mo, F. v. d. Bosch and S. White, *Galaxy Formation and Evolution* (Cambridge University Press, Cambridge, England, 2010).
- [29] M. Takada, E. Komatsu and T. Futamase, Phys. Rev. D **73**, 083520 (2006).
- [30] L. Wang and P. J. Steinhardt, Astrophys. J. **508**, 483 (1998); E. V. Linder and A. Jenkins, Mon. Not. Roy. Astron. Soc. **346**, 573 (2003).
- [31] A. Jenkins, C. S. Frenk, S. D. M. White, J. M. Colberg, S. Cole, A. E. Evrard, H. M. P. Couchman and N. Yoshida, Mon. Not. Roy. Astron. Soc. **321**, 372 (2001).
- [32] R. K. Sheth, H. J. Mo and G. Tormen, Mon. Not. Roy. Astron. Soc. **323**, 1 (2001); R. K. Sheth and G. Tormen, Mon. Not. Roy. Astron. Soc. **329**, 61 (2002).
- [33] W. H. Press and P. Schechter, Astrophys. J. **187**, 425 (1974).
- [34] S. Sasaki, Publ. Astron. Soc. Jap. **46**, 427 (1994); E. Ripamonti, Mon. Not. Roy. Astron. Soc. **376**, 709 (2007); S. Mitra, G. Kulkarni, J. S. Bagla and J. K. Yadav, Bull. Astron. Soc. Ind. **39**, 1,(2011).
- [35] W. H. Press, S. A. Teukolsky, W. T. Vetterling and B. P. Flannery, *Numerical Recipes in Fortran 90*, Second edition (Cambridge University Press, Cambridge, England, 1996).
- [36] See, <http://www.mpa-garching.mpg.de/~komatsu/CRL/index.html>.
- [37] See, for instance, <http://www.nag.com/> and <http://www.netlib.org/>.
- [38] F. Finelli, J. Hamann, S. M. Leach and J. Lesgourgues, JCAP **04** 011 (2010).
- [39] M. Benetti, S. Pandolfi, M. Lattanzi, M. Martinelli and A. Melchiorri, [arXiv:1210.3562](https://arxiv.org/abs/1210.3562) [astro-ph.CO].